




Rapid onset of molecular friction in liquids bridging between the atomistic and hydrodynamic pictures

Arthur V. Straube ^{1,2}, Bartosz G. Kowalik³, Roland R. Netz ³ & Felix Höfling ^{1,2}✉

Friction in liquids arises from conservative forces between molecules and atoms. Although the hydrodynamics at the nanoscale is subject of intense research and despite the enormous interest in the non-Markovian dynamics of single molecules and solutes, the onset of friction from the atomistic scale so far could not be demonstrated. Here, we fill this gap based on frequency-resolved friction data from high-precision simulations of three prototypical liquids, including water. Combining with theory, we show that friction in liquids emerges abruptly at a characteristic frequency, beyond which viscous liquids appear as non-dissipative, elastic solids. Concomitantly, the molecules experience Brownian forces that display persistent correlations. A critical test of the generalised Stokes–Einstein relation, mapping the friction of single molecules to the visco-elastic response of the macroscopic sample, disproves the relation for Newtonian fluids, but substantiates it exemplarily for water and a moderately supercooled liquid. The employed approach is suitable to yield insights into vitrification mechanisms and the intriguing mechanical properties of soft materials.

¹Freie Universität Berlin, Department of Mathematics and Computer Science, Arnimallee 6, 14195 Berlin, Germany. ²Zuse Institute Berlin, Takustraße 7, 14195 Berlin, Germany. ³Freie Universität Berlin, Department of Physics, Arnimallee 14, 14195 Berlin, Germany. ✉email: f.hoeffling@fu-berlin.de

Molecular friction is a key ingredient for dynamic processes in fluids: it limits diffusion, governs dissipation, and enables the relaxation towards equilibrium. In a liquid environment, the friction experienced by solvated molecules and nanoprobe exhibits a delayed response to external stimuli, indicating non-Markovian dynamics^{1–4}. Such memory is found on sub-picosecond up to microsecond scales; it has repercussions on macromolecular transition rates^{5–7} and is manifest in the visco-elastic behaviour of soft materials^{8–11}. However, the origin of friction from conservative forces between molecules and atoms remains as one of the grand challenges of the physics of fluids^{12–14}.

Stokes's friction law, describing the resistance to a steadily dragged immersed sphere of radius a , links the friction ζ_0 to the (macroscopic) shear viscosity η_0 , and the relation $\zeta_0 = 6\pi\eta_0 a$ scales down remarkably well to single molecules^{15,16}. Stokes's hydrodynamic treatment¹⁷ from 1851 was actually more general and addressed slow oscillatory motions in viscous fluids, motivated by inaccuracies of pendulum clocks caused by air flow (Fig. 1a). These predictions of a dynamic friction $\zeta(\omega)$ that depends on the oscillation frequency ω have been interpreted in terms of a delayed response, also referred to as hydrodynamic memory, and have only recently been shown to be quantitative also for micron-sized particles^{1,2}. In the domain of micro-rheology, measurements of $\zeta(\omega)$ are used to infer the mechanical properties of complex fluids^{18–22}.

From the perspective of individual molecules or atoms, fluids are governed by conservative interactions and obey Newton's equations of motion, yielding smooth and time-reversible trajectories (Fig. 1b, c). In particular, a single molecule is not subject to friction in this picture, and the mechanism of the required entropy production is far from obvious. Macroscopic friction and other transport coefficients have been linked to microscopic chaos and the Lyapunov spectrum of the liquid^{23–25}, yet the connection of the latter to the corresponding Green–Kubo integrands, or equivalently, to the dynamic friction $\zeta(\omega)$, is an open issue²⁴. First-principle theories to friction are hampered by the fact that liquids are strongly interacting systems. An insightful, formal relation between the many-particle Liouville operator and dissipation spectra was derived in the seminal works by Zwanzig, Mori, and others^{26,27}, but the analytic evaluation of the resulting expressions hinges on uncontrolled approximations. For example, a systematic short-time expansion of the motion at all orders would yield zero friction (see “Methods”). Early work on

dissipation spectra recognised the importance of exact sum rules^{28,29}, the proposed ad hoc models, however, violate the sum rules at higher orders. Theoretical progress was made for hard-sphere fluids, where billiard-like collisions generate an instantaneous, Markovian contribution to friction³⁰, thereby rendering the frictionless regime inaccessible.

To gradually bridge between the atomistic and hydrodynamic regimes, one would ideally like to have a magnifying glass that allows for zooming from the slowest to the fastest processes, thus obtaining an increasingly sharper view of the molecular details (Fig. 1a). Spectral quantities such as $\zeta(\omega)$ can serve this purpose with the frequency ω as the control knob. Implementing this idea in simulations of liquids and numerically tracing the friction of molecules over wide frequency windows from fully developed dissipation all the way down to the non-dissipative regime would reveal sizable variations of $\zeta(\omega)$. Such deviations of $\zeta(\omega)$ from a constant friction ζ_0 signify non-Markovian motion that is widely cast in the generalised Langevin equation [“Methods”, Eq. (1)], parametrised by an associated memory function $\gamma(t)$. The quantities $\zeta(\omega)$ and $\gamma(t)$ are related to each other by a cosine transform, but the determination of either of them from data is a formidable challenge, with substantial progress in the past years^{31–38}. Reaching the high-frequency regime was precluded so far by practical limitations, e.g., statistical noise and insufficient dynamic windows.

Here, we have overcome these limitations by high-precision simulations and an advanced data analysis that utilises physical principles. For three distinct liquids—water, a dense Lennard–Jones (LJ) fluid representing a simple, mono-atomic liquid, and a supercooled binary mixture serving as a model glass former—we obtained low-noise, cross-validated data for the dynamic friction $\zeta(\omega)$ and the frequency-dependent viscosity $\hat{\eta}(\omega)$ over windows that span from the fastest to the slowest processes in each liquid. Corroborated by these data, we give rigorous arguments that dissipative processes in molecular liquids are exponentially fast suppressed as frequency is increased. As a consequence, the liquid's response is purely elastic above a characteristic frequency ω_c , a feature that goes beyond popular models of friction and viscoelasticity. Furthermore, the magnitude of friction cannot be inferred from the instantaneous behaviour of molecular trajectories: its origin is non-local in time. Finally, having data available for both $\zeta(\omega)$ and $\hat{\eta}(\omega)$, we tested the connection between microscopic friction and the macroscopic mechanical properties of complex fluids, postulated by the generalised Stokes–Einstein

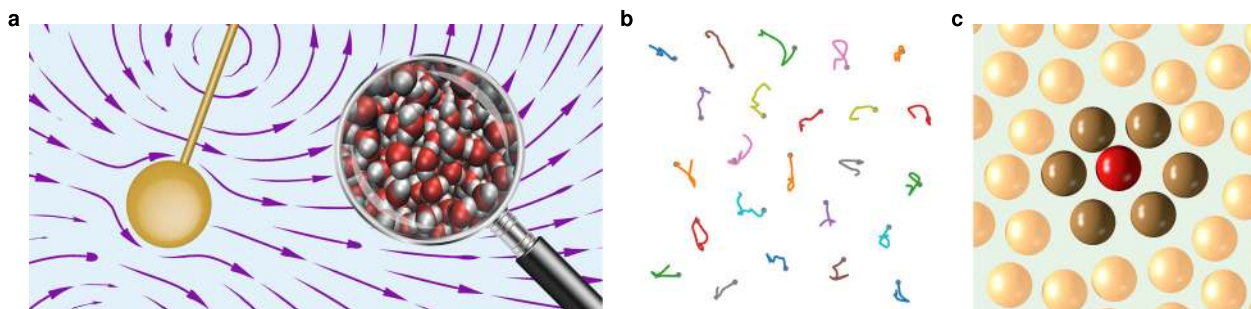


Fig. 1 Dynamic friction bridges between the hydrodynamic and atomistic pictures of liquids. **a** A pendulum that oscillates in a viscous fluid with frequency ω experiences a dynamic friction $\zeta(\omega)$ as calculated by Stokes (1851) for slow motion. The associated flow pattern (stream lines) leads to hydrodynamic memory of the motion. Magnifying the microscopic scale, the fluid consists of molecules that obey Newton's equations, which are non-dissipative and generate smooth trajectories. Stokes's result for the pendulum scales down to single molecules, and the function $\zeta(\omega)$ provides the bridge between the frictionless (microscopic) and the hydrodynamic (macroscopic) descriptions. **b, c** In liquids, the short-time trajectories of molecules (**b**) are smooth, but chaotic curves due to molecules rattling in transient cages formed by their neighbours (**c** brown spheres). The onset of friction is driven by the momentum transfer to the cage, as supported by control simulations of a single particle (red sphere) in a matrix of pinned particles (brown and yellow). Illustration for a mono-atomic fluid in two dimensions.

relation. The latter is found to either fail completely (mono-atomic liquid), serve as a qualitative description (water), or being a nearly quantitative relation (supercooled liquid).

Results

Molecular friction in liquids emerges rapidly. Instead of observing the response to an oscillatory force, we recorded the Brownian position fluctuations in equilibrium and link them to the friction, taking advantage of a fluctuation–dissipation relation. For the three liquids under investigation, we carried out molecular dynamics simulations to compute the mean-square displacement (MSD). Using the MSD as sole input, we estimated both the dynamic friction $\zeta(\omega)$ and the memory function $\gamma(t)$ in an ansatz-free approach, following two complementary routes

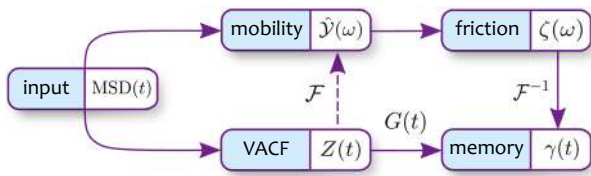


Fig. 2 Flow chart of the data analysis. Along the upper route, one starts from the mean-square displacement (MSD) and computes the generalised mobility $\hat{Y}(\omega)$ by numerical differentiation and a suitable Fourier transform \mathcal{F} (adapted Filon algorithm, Eq. (22)); the dynamic friction $\zeta(\omega)$ follows via Eq. (7). A Fourier backtransform then yields the memory function $\gamma(t)$. The latter can be obtained more directly along the lower route, which is based on the velocity autocorrelation function (VACF) $Z(t)$ and employs a deconvolution in time domain (Eq. (23)).

that allow for cross-validation (see Fig. 2 and “Methods”). The first route invokes complex analysis and is based on the Fourier–Laplace transform of correlation functions, sampled on a sparse time grid (“adapted Filon algorithm”). Second and independently, we computed the antiderivative of $\gamma(t)$ using a stable deconvolution technique for uniform time grids.

Although all three liquids display rather different dynamics, leaving distinct fingerprints in their friction spectra, their high-frequency behaviours of $\zeta(\omega)$ share significant similarities (Fig. 3a–c). Most remarkably, the data demonstrate that beyond a liquid-characteristic frequency, $\omega \gtrsim \omega_c$, the friction $\zeta(\omega)$ goes exponentially fast to zero. Such a rapid spectral variation has to be contrasted to the typical algebraic peaks, i.e., the Lorentz–Debye shape, and we argue in the following that our finding is generic for molecular fluids. Upon decreasing frequency, the onset of friction is followed by liquid-specific behaviour over several decades in time until the hydrodynamic value ζ_0 is established: in water, our results for the friction $\zeta(\omega)$ exhibit a local maximum at $\omega/2\pi \approx 5$ THz, followed by a slow increase towards the limiting value ζ_0 , which is reached near frequencies of 0.1 THz. For the LJ fluid, $\zeta(\omega)$ varies more smoothly with a global maximum at an intermediate frequency, and ζ_0 is approached slowly from above in accord with the hydrodynamic square-root singularity [Eq. (18)], essentially calculated by Stokes already¹⁷. On theoretical grounds, this feature of $\zeta(\omega)$ is generic for all liquids, yet it is suppressed in our data for the other two liquids due to a small prefactor. In the supercooled liquid, we observe a scale separation by three dynamic decades of (i) the rapid onset of friction and (ii) the slow emergence of the hydrodynamic limit. The second process is associated with cage relaxation, strongly delayed in the glassy state, which suggests that the driving mechanism behind

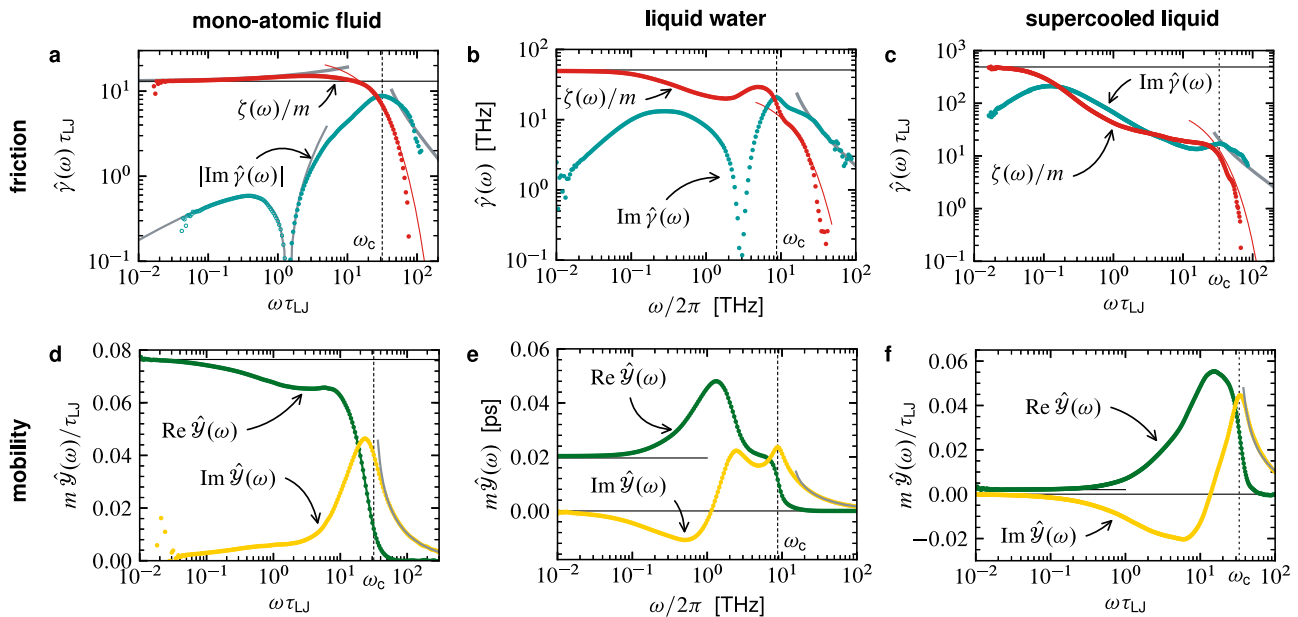


Fig. 3 Dynamic friction and generalised mobility of three prototypical liquids. Columns show simulation results for a mono-atomic fluid, liquid water, and a supercooled liquid, obtained from the data analysis depicted in Fig. 2, with the mean-square displacement (MSD, not shown) as initial input. **a–c** The dynamic friction (red) is the real part of the memory kernel $\hat{\gamma}(\omega)$, as computed from Eq. (6). It interpolates between the hydrodynamic value ζ_0/m (horizontal lines) and a rapid decrease to zero at high frequencies ($\omega \gg \omega_c$); thin red lines mark exponential decays, $\sim e^{-\omega/\omega_c}$, to guide the eye. In case of the Lennard-Jones fluid (**a**), $\zeta(\omega)$ is consistent with Stokes’s small- ω asymptote [grey line, Eq. (18)], with parameters taken from a fit to the long-time tail of $Z(t)$ (inset of Fig. 4a). The elastic response $\text{Im} \hat{\gamma}(\omega)$ (turquoise) exhibits a local maximum at high frequencies, defining the characteristic frequency ω_c (vertical lines), and follows the high-frequency asymptote [Eq. (15), grey line], with all parameters fixed by short-time fits to the MSD data. The frequency ω_c is close to, but different from the Einstein frequency ω_0 . **d–f** Numerical results for the generalised mobility $\hat{Y}(\omega)$, which describes the response to an applied small, oscillatory force (see “Methods”). The real part $\text{Re} \hat{Y}(\omega)$ (green) approaches the hydrodynamic mobility $1/\zeta_0$ (horizontal lines) as $\omega \rightarrow 0$ and vanishes rapidly at large frequencies. The imaginary part (yellow) encodes the elastic response, which has a resonance near ω_c (vertical lines); at larger frequencies, the data match with theoretical predictions [grey lines, Eq. (14)].

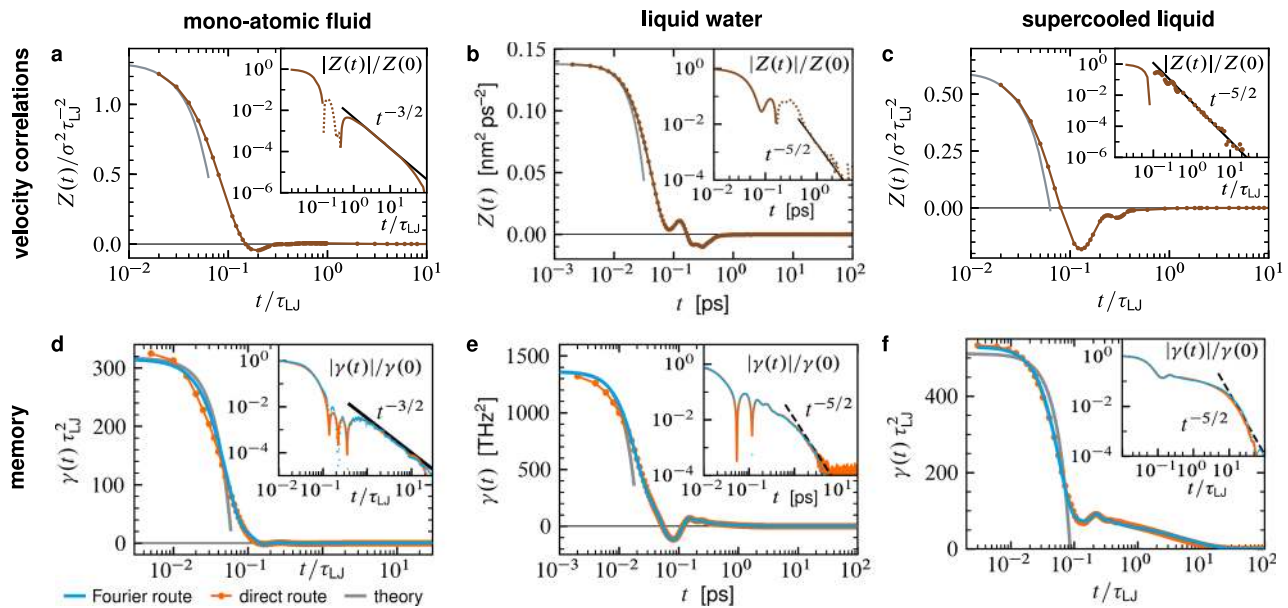


Fig. 4 Velocity autocorrelators and corresponding memory functions for the three investigated liquids. Columns show results for a mono-atomic fluid, liquid water, and a supercooled liquid. **a–c** simulation results for the velocity autocorrelation function (VACF, brown symbols) display a parabolic decrease at short times (grey lines) and power-law decays at long times (insets, negative values are dotted). The VACF is obtained from the second derivative of the mean-square displacement with respect to lag time. **d–f** The memory function $\gamma(t)$ encodes the autocorrelation of Brownian forces on the molecules (Eq. (2)). For each liquid, $\gamma(t)$ was computed from a cosine transform of $\hat{\zeta}(\omega)$ [blue lines, Eq. (9)] with input data from Fig. 3a–c) and is compared to the deconvolution results in time domain [orange lines, Eq. (23)]. The data follow the predicted short-time decay Eq. (16) (grey lines) and exhibit power-law decays consistent with Eq. (19) (insets), preceded by an ultra-slow decay in case of the supercooled liquid (f).

the onset of friction is not in the structural relaxation of the fluid. Close to the glass transition, the small-frequency friction ζ_0 is governed by self-similar relaxation processes and obeys asymptotic scaling laws^{39,40}; the magnitude (prefactor) of these laws, however, is set at high frequencies.

Friction depends on the coupling of fast and slow processes.

The obtained data of $\zeta(\omega)$ cover the full range of the dynamic response, thereby connecting physics at different scales. Before discussing the remaining panels (d–f) of Fig. 3, we rationalise key features of $\zeta(\omega)$ by tracing their origins to the dynamics of the fluid particles at short and long times (going backwards in Fig. 2). The relevant properties are prominently visible in the second derivative of the MSD, the velocity autocorrelation function (VACF), $Z(t) := \partial_t^2 \text{MSD}(t)/6$, after numerical differentiation with respect to the lag time t (Fig. 4a–c). The following should be contrasted to Ornstein’s model for Brownian motion, employing a single exponential decay of velocity correlations, $Z(t) \approx v_{\text{th}}^2 \exp(-\zeta_0 t/m)$, which implies a constant (Markovian) friction, $\zeta(\omega) \approx \zeta_0$; by v_{th} we denote the thermal velocity, and m is the molecular mass. As a distinct feature of molecular fluids, obeying Newton’s equations, the VACF’s true short-time decay is parabola-shaped¹⁶, $Z(t \rightarrow 0) \approx v_{\text{th}}^2 (1 - \omega_0^2 t^2/2)$, introducing the Einstein frequency ω_0 . For dense liquids, the VACF, after a sign change, generically displays a regime of anti-correlations, which reflect the transient caging by neighbouring molecules (Fig. 1c). For water and the supercooled liquid, these anti-correlations relax slowly with an intermediate power-law decay, $Z(t) \sim -t^{-5/2}$ (insets of Fig. 4b, c); such a decay was observed earlier in supercooled liquids^{41,42} and it is a well-established long-time tail in colloidal suspensions^{43–45} and for diffusion in an arrested, disordered environment^{46,47}.

The famous long-time tail encoding hydrodynamic memory^{16,48,49}, $Z(t \rightarrow \infty) \sim t^{-3/2}$, is clearly developed in our data for the LJ fluid after another sign change (inset of Fig. 4a), and in

this situation, Stokes’s hydrodynamics describes the slow motion of single molecules (Fig. 3a). For the other two liquids studied, the tail is not visible in our data due to a small prefactor, which following mode-coupling arguments decreases as either viscosity or diffusivity increases¹⁶.

The dynamic friction is closely linked to the complex-valued, generalised mobility $\hat{Y}(\omega)$ via $\zeta(\omega) = \text{Re}[\hat{Y}(\omega)^{-1}]$. This mobility encodes the response to a small, oscillatory force and is accessible in, e.g., scattering experiments⁵⁰. Here, we computed $\hat{Y}(\omega)$ from the VACF upon employing a fluctuation–dissipation relation (see “Methods” and Fig. 3d–f). Our data reveal a generic, rapid decrease of the dissipative part, $\hat{Y}'(\omega) := \text{Re} \hat{Y}(\omega)$, upon increasing frequency towards the microscopic regime, $\omega \gg \omega_c$; concomitantly, the elastic response, $\hat{Y}''(\omega) := \text{Im} \hat{Y}(\omega)$, has a resonance near ω_c due to vibrational motion of molecules in their cages. In the low-frequency limit, the reciprocal of the macroscopic friction is recovered, $\hat{Y}(\omega \rightarrow 0) = 1/\zeta_0$. In the examples studied, both regimes are separated by at least two decades in time, which show material-specific features: the mobility of water molecules is 2.5-fold enhanced over its macroscopic value near $\omega/2\pi \approx 1.3$ THz; similarly, a factor of 30 is observed for the supercooled liquid. At variance, the hydrodynamic long-time tail, as for the LJ liquid, demands $\hat{Y}'(\omega \rightarrow 0)$ to be approached from below. The interplay of slow and fast processes enters the response $\hat{Y}(\omega)$, and thus the dynamic friction $\zeta(\omega)$, at all frequencies, which is borne out by the Kramers–Kronig relations. In particular, non-analytic behaviour of $\hat{Y}'(\omega)$ as $\omega \rightarrow 0$ influences the detailed onset of friction at large frequencies.

The origin of friction is non-local in time. The rapid decrease of $\hat{Y}'(\omega)$ is mathematically justified from the short-time properties of the VACF. Physical molecular trajectories, being solutions to Newton’s equations, are smooth and yield a smooth function $Z(t)$;

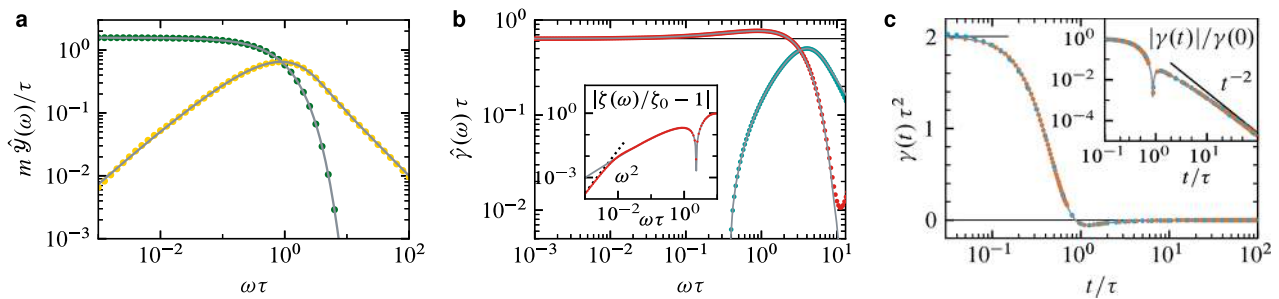


Fig. 5 Theoretical model justifies exponentially fast onset of friction and persistent memory. Exact results (grey solid lines) for the model of $Z(t)$ in Eq. (20), combining the smoothness and time-reversal symmetry of molecular autocorrelation functions with a long-time tail. As a sensitive test of our numerical procedures, symbols show numerical results from the mean-square displacement as input, sparsely sampled on a geometrically spaced grid. The panels show **a** the complex-valued, generalised mobility $\hat{Y}(\omega)$, **b** the dynamic friction $\zeta(\omega)$ and its elastic counterpart $\text{Im} \hat{y}(\omega)$, and **c** the memory function $\gamma(t)$ in time domain. The latter inherits the long-time tail $\sim t^{-2}$ from the velocity autocorrelation function, but of opposite sign (inset). The tail induces non-analytic behaviour of $\zeta(\omega)$ at small frequencies, which crosses over to $\sim \omega^2$ due to the smooth, exponential cutoff of the Fourier integrals (inset of panel **b**). Same colour code as in Figs. 3 and 4.

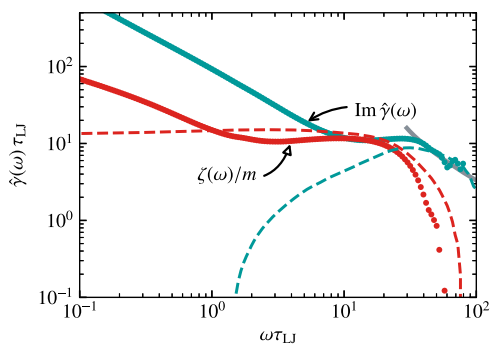


Fig. 6 Friction emerges due to rattling motion in immobile cages.

Dynamic friction $\zeta(\omega)$ (red symbols) obtained in a control simulation of a single particle moving in a frozen-in cage formed by neighbouring particles (Fig. 1c). The setup was created by pinning the particles of the Lennard-Jones fluid except for one; results correspond to an ensemble average over 10^6 typical cages. The imaginary part of the memory kernel $\hat{y}(\omega)$ (turquoise) ties in with the high-frequency prediction (grey). Dashed lines show the results for the unconstrained fluid at the same conditions for comparison (Fig. 3a).

in particular, all derivatives $Z^{(n)}(t)$ exist at $t=0$ and are finite. Thus, invoking exact sum rules [Eq. (10)], all moments of the spectrum $\hat{Y}(\omega)$ are finite, which requires an exponentially fast decay as $\omega \rightarrow \infty$. (This is a special case of a more general characterisation of exponentially decaying probability measures⁵¹.) Combining with the large- ω asymptote of the imaginary part, $\hat{Y}''(\omega) \simeq 1/m\omega \gg \hat{Y}'(\omega)$ (see “Methods”) and using $\zeta(\omega) = \hat{Y}'(\omega)/[\hat{Y}'(\omega)^2 + \hat{Y}''(\omega)^2]$ proves that $\zeta(\omega) \simeq (m\omega)^2 \hat{Y}'(\omega)$ as $\omega \rightarrow \infty$ and thus an exponentially fast suppression of the friction. We stress further that such behaviour is not contained in representations of $\zeta(\omega)$ as a truncated continued fraction^{16,52}.

It is tempting to use a systematic short-time expansion of $Z(t)$ to predict the large-frequency behaviour of the friction. However, $Z(t)$ being an even function due to time-reversal symmetry in equilibrium renders the large- ω asymptotes zero, $\hat{Y}'(\omega) \equiv 0$ and thus $\zeta(\omega) \equiv 0$, even if the complete Taylor series of $Z(t)$ in $t=0$ was known (see “Methods”). Note that $\hat{Y}''(\omega)$ and the elastic counterpart of $\zeta(\omega)$ are well captured by such an expansion (Fig. 3d–f). This observation underlines that, on all scales, friction emerges as a phenomenon that is non-local in time, i.e., it cannot be anticipated from the local behaviour of the molecular trajectories.

Our numerical and theoretical findings are supported by an analytically solvable example. The choice $Z(t) = v_{\text{th}}^2 [1 + (t/\tau)^2]^{-1}$ combines the smoothness and time-reversal symmetry of molecular autocorrelation functions with a long-time tail. It yields an exponential decay of the mobility, $\hat{Y}'(\omega) = (\pi\tau/2m) e^{-|\omega\tau|}$ (dissipative part), and hence a rapid suppression of friction, $\zeta(\omega \rightarrow \infty) \sim (\omega\tau)^2 e^{-\omega\tau}$, as demanded above (see “Methods” and Fig. 5).

Irreversible momentum transfer drives the onset of friction. A pressing question is about the physical mechanism that generates the onset of friction. Motivated by our results for the supercooled liquid (Fig. 3c), we performed a control simulation for the LJ fluid with the structural relaxation switched off by pinning all particles but one. The rattling motion in such a frozen-in cage (Fig. 2) experiences a dynamic friction that closely resembles our generic findings for $\zeta(\omega)$ at high frequencies, $\omega \gtrsim \omega_c$ (Fig. 6). Upon decreasing frequency from ω_c to zero, the two dynamics deviate strongly as is most evident in the elastic response: whereas $\text{Im} \hat{y}(\omega)$ decreases for the unconstrained fluid and exhibits a zero crossing enforced by hydrodynamics [Eq. (17) and Fig. 3a], it remains positive for the pinned case and grows as $\text{Im} \hat{y}(\omega \rightarrow 0) \sim 1/\omega$, reminiscent of what one obtains for an Ornstein–Uhlenbeck (OU) particle in a harmonic trap¹. For even smaller frequencies, $\omega \lesssim \tau_{LJ}^{-1}$, the dissipation diverges too, approximately as $\zeta(\omega \rightarrow 0) \sim \omega^{1/2}$, which we attribute to the irregular shape of the confining cages; for the OU model with harmonic confinement, $\zeta(\omega) \simeq \text{const}$. At high frequencies, however, the confinement is not relevant, and we conclude that it is the fast, yet irreversible momentum transfer to neighbouring molecules that drives the onset of friction. This is corroborated by the observation that instantaneous momentum exchange implies a non-zero limit, $\zeta(\omega \rightarrow \infty) > 0$, as in the case of hard spheres³⁰. The fact that dissipation is linked to trajectories for which the time-reversed path is extremely improbable leads us to speculate that the onset frequency ω_c is intimately related to the largest Lyapunov exponent λ_{max} of the fluid, which is close to, but different from the Einstein frequency ω_0 (Posch & Hoover²⁵).

Dynamic friction implies intricate memory of Brownian motion. Within the framework of the generalised Langevin equation [Eq. (1)], momentum relaxation is governed by a memory function $\gamma(t)$ that is fully determined by $\zeta(\omega)$ [Eqs. (7) and (9)]. At the same time, $\gamma(t)$ is also the autocorrelator of Brownian, random forces on the molecules, up to a constant

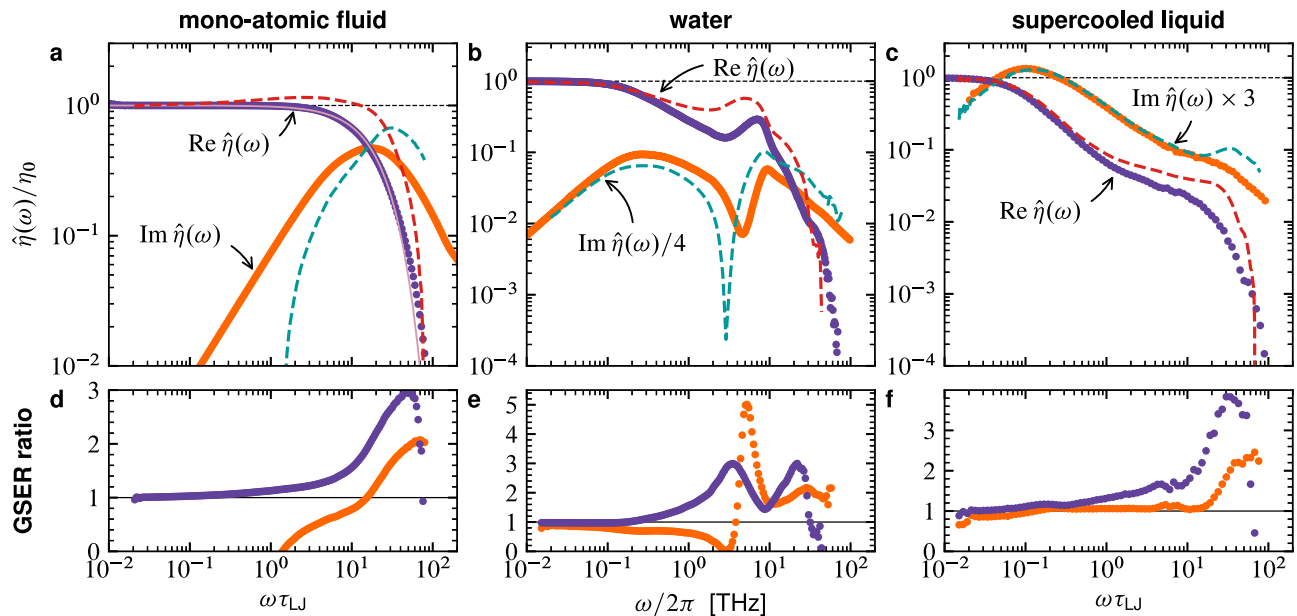


Fig. 7 Test of the generalised Stokes-Einstein relation (GSER). **a–c** The generalised viscosity $\text{Re } \hat{\eta}(\omega)$ (violet symbols) of the three liquids under investigation (columns) is compared to the GSER prediction $\zeta(\omega)/6\pi a$ (red dashed lines), based on the dynamic friction data of single molecules (Fig. 3a, c), and correspondingly for the imaginary counterparts of the elastic responses (orange symbols and turquoise dashed lines). The effective particle radius a for each liquid is chosen such that the viscosity and friction curves coincide at $\omega = 0$. The pink solid line in **a** is an empirical fit of a compressed exponential, $\text{Re } \hat{\eta}(\omega) \simeq \eta_0 \exp(-(\omega/\omega_\eta)^\beta)$ with $\beta = 1.29$ and $\omega_\eta = 1.19 \omega_0$. In **b, c** the data for the elastic responses are shifted by the indicated factors for clarity. **d–f** The GSER is tested by plotting the ratios $\zeta(\omega)/6\pi[\text{Re } \hat{\eta}(\omega)]a$ (violet) and $m[\text{Im } \hat{\eta}(\omega)]/6\pi[\text{Im } \hat{\eta}(\omega)]a$ (orange); deviations from unity quantify the GSER violation.

prefactor, and $\zeta(\omega)$ encodes the corresponding spectrum [Eq. (2)]. Within Ornstein’s idealised model of Brownian motion, one assumes independent Brownian forces, implying a flat, white spectrum, $\zeta(\omega) \simeq \zeta_0$, and a delta-peaked memory function $\gamma(t)$. For molecular liquids, however, the memory functions display a universal parabola-shaped short-time decay [Fig. 4d–f and Eq. (16)]. For water and the LJ fluid, the short-time regime of $\gamma(t)$ is followed by oscillatory behaviour including sign changes and, finally, different power-law decays for the two liquids encoding different physics (insets of Fig. 4d, e also see Fig. 5c); generally, power-law tails of the memory function are directly inherited from the VACF without a change of exponent [Eq. (19)]. For the supercooled liquid, $\gamma(t)$ remains positive and exhibits the onset of a plateau (near $t \approx 0.3\tau_{LJ}$), which decays logarithmically slowly over 2 decades in time (Fig. 4f). From the modelling perspective, it is desirable to approximate the memory functions such that the initial decay, the typical persistence time, and the integral of $\gamma(t)$ are reproduced, the latter yielding ζ_0 [Eq. (13)]. For all three liquids, the complexity and the long-lived nature of the memory, however, preclude simple models of $\gamma(t)$ such as the superposition of few exponential decays. The quantitative knowledge of $\zeta(\omega)$, as obtained here, paves the way for more favourable approximations of memory in the frequency domain, which can yield mathematically and physically consistent interpolations of Brownian motion from the fastest to the slowest scales.

Discussion

Based on theoretical arguments and corroborated by simulation data that cover up to three orders in magnitude and 4 decades in frequency, we have shown that the friction $\zeta(\omega)$ in molecular liquids emerges rapidly at a large, liquid-specific frequency ω_c from the time-reversible motion of the atoms. This onset of friction is driven by the irreversible momentum transfer to neighbouring molecules, but also influenced by the slowest processes at hydrodynamic scales. The exponentially fast decay of

dissipation spectra such as $\zeta(\omega)$ is easily shadowed by approximations, and as a modelling constraint it is under-investigated in the existing microscopic theories of liquids. The observation that the high-frequency behaviour of $\zeta(\omega)$ is reproduced by the motion of a single particle in an immobile cage refines the question on the quantitative link between friction and microscopic chaos. Concretely: whether and how does the frequency dependence of transport coefficients relate to the Lyapunov spectrum of the liquid^{23,24}?

Going beyond the dynamics of single molecules and their friction, the relation to the visco-elastic properties of complex fluids is of ongoing interest for the physics of polymers, living cells, and the glass transition. The potentially tight coupling between single-particle and collective responses was phrased as an ad hoc extension of Stokes’s friction law to the frequency domain, $\zeta(\omega) = 6\pi \text{Re}[\hat{\eta}(\omega)]a$, referred to as generalised Stokes–Einstein relation (GSER), which has found wide applications in the context of microrheology experiments^{18–21}. It links the dynamic friction $\zeta(\omega)$ of a probe particle to the dynamic shear modulus, $\hat{G}(\omega) = -i\omega\hat{\eta}(\omega)$, a complex-valued function encoding the stress response of the macroscopic fluid sample to a small, oscillatory shear strain. The generalised viscosity $\hat{\eta}(\omega)$ tends to the hydrodynamic shear viscosity η_0 as $\omega \rightarrow 0$, with $\text{Re } \hat{\eta}(\omega)$ representing the spectrum of shear stress fluctuations (up to a constant factor) by a fluctuation–dissipation relation. Thus, if the GSER holds the single-particle memory $\gamma(t)$ is proportional to the autocorrelator of shear stresses, which means that the Brownian force on the particle and the fluctuation of the shear stress are statistically equivalent variables.

A critical assessment of the validity of the GSER is permitted by comparing our data for $\zeta(\omega)$ to results for $\hat{\eta}(\omega)$, calculated within the same simulations (see Fig. 7 and “Methods”). Generically, the dissipative part, $\text{Re } \hat{\eta}(\omega)$, decays exponentially fast as $\omega \rightarrow \infty$, which is required by analogous arguments as given for $\zeta(\omega)$ and $\mathcal{J}^\nu(\omega)$. For high frequencies, only the imaginary part

survives due to its slow decay, $\hat{\eta}(\omega) \simeq G_\infty/(-i\omega)$, inducing a non-zero and real-valued modulus, $\hat{G}(\omega \gg \omega_c) \approx G_\infty > 0$. Therefore, our data clearly demonstrate that, indeed, liquids respond to high-frequency shear like a non-dissipative, elastic solid as put forward by the classical work of Frenkel⁵³. However, the attempt to predict the elastic modulus G_∞ from the vibrational motion of molecules in their cages, by virtue of the GSER, would considerably overestimate the modulus by factors of ≈ 2 for the three liquids studied (Fig. 7d–f). In passing, we note that Maxwell’s model for viscoelasticity^{16,52,53}, $\hat{\eta}(\omega) = G_\infty \tau / (1 - i\omega\tau_M)$ with some relaxation time τ_M , breaks down at high frequencies as it implies a slowly decaying real part, $\text{Re} \hat{\eta}(\omega \rightarrow \infty) \sim \omega^{-2}$, in sharp contrast to exact sum rules²⁸ and to the exponentially fast decay for molecular liquids. Therefore, treatments of sound-like, elastic waves on the footing of this and similar models appear incomplete.

The passage from the elastic to the viscous limit occurs upon decreasing frequency, leading in case of the LJ fluid to a monotonic increase of $\text{Re} \hat{\eta}(\omega)$, which, empirically, follows a compressed exponential over almost the full frequency domain (Fig. 7a). In particular, $\hat{\eta}(\omega) \approx \eta_0$ is constant for $\omega \lesssim 2\tau_{LJ}^{-1}$, which defines the hydrodynamic regime. For these frequencies, the single-molecule response is very well described by Stokes’s dynamic friction [Eq. (18)], making the GSER violation apparent for Newtonian fluids, for which $\hat{\eta}(\omega) = \eta_0$. It is evidenced further by the dissimilarity of the elastic parts, $\text{Im} \hat{\gamma}(\omega)$ and $\text{Im} \hat{\eta}(\omega)$.

For water, the viscosity and friction spectra share similar features and coincide fairly well (Fig. 7b), including the elastic parts. Thus, the GSER serves as a reasonable qualitative description, in particular for frequencies below ≈ 2 THz, i.e., slower than the vibrations of the first hydration shell⁵⁴. In supercooled liquids, the Stokes–Einstein relation for molecules (i.e., the GSER for $\omega \rightarrow 0$) holds in the presence of a huge variation of the viscosity. In particular, the ratio ζ_0/η_0 is observed to be constant over a wide temperature range—in line with the mode-coupling theory of the idealised glass transition⁴⁰. At very low temperatures, however, marked deviations from the Stokes–Einstein relation (mostly studied for $\omega \rightarrow 0$) have received considerable attention as they signify the opening of additional relaxation channels not included in the standard theory^{55–59}. For the moderately supercooled liquid studied here exemplarily, both viscous and elastic responses satisfy the GSER over a wide frequency window (Fig. 7c). Notably, the elastic components collapse almost perfectly in this case, $\text{Im} \hat{\gamma}(\omega) \sim \text{Im} \hat{\eta}(\omega)$, which we attribute to the same (apparent) power-law scaling, $\approx \omega^{-0.75}$, at intermediate frequencies. Yet, the collective response lacks the elastic peak of $\text{Im} \hat{\gamma}(\omega)$ at ω_c , causing the breakdown of the GSER at large frequencies. This suggests that a future frequency-resolved study of systematic deviations from the GSER upon further supercooling can clarify the separate contributions of fast and slow processes to the decoupling of diffusion and viscosity (“Stokes–Einstein violation”) close to the glass transition temperature.

We conclude that molecular friction in liquids arises from a complex interplay of processes on very disparate time scales. The large variability of $\zeta(\omega)$ observed over orders of magnitude reveals the strongly non-Markovian nature of Brownian motion in any liquid environment, with far-reaching implications for nanoscale processes. Examples are as diverse as reaction rates and barrier crossings in macromolecular dynamics^{5–7} and flows near liquid–solid interfaces^{44,60–62}; the ability to quantify the corresponding memory is vital for their realistic descriptions. From a numerical point of view, our ansatz-free approach has immediate applications to and extends current methods^{37,38} for the analysis of high-resolution microrheology data^{1–3,21}, which involves deducing frequency-dependent moduli from the displacement statistics along the same lines as done here for the dynamic

friction. Relying merely on the existence of a steady state [Eq. (12)], the developed methodology is not limited to friction, but can be transferred to the analysis of non-Markovian time series from simulation and experiment. It finds novel uses in, e.g., the anomalous diffusion within living cells¹¹ and the kinetics of chemical reactions⁶³. It opens a promising avenue for research on the migration of malignant cells in tissue⁶⁴ and on predictive stochastic models of financial market⁶⁵ and geographic⁶⁶ data.

Methods

Generalised Langevin equation. A labelled fluid particle of mass m , position $\mathbf{r}(t)$, and momentum $\mathbf{p}(t) = m\dot{\mathbf{r}}(t)$ obeys the generalised Langevin equation (GLE)⁶⁷:

$$\dot{\mathbf{p}}(t) = - \int_0^t ds \gamma(t-s) \mathbf{p}(s) + \boldsymbol{\xi}(t), \quad (1)$$

where the Brownian force $\boldsymbol{\xi}(t)$ is a stochastic process with zero mean and covariance

$$\langle \boldsymbol{\xi}(t) \otimes \boldsymbol{\xi}(t') \rangle = mk_B T \gamma(|t-t'|) \mathbf{1} \quad (2)$$

to satisfy the fluctuation–dissipation theorem. Rewriting Eq. (1) for the the velocity autocorrelation function (VACF), $Z(t) = \langle \mathbf{p}(t) \cdot \mathbf{p}(0) \rangle / (3m^2)$, describing momentum relaxation, yields

$$\dot{Z}(t) = - \int_0^t ds \gamma(t-s) Z(s), \quad Z(0) = \frac{k_B T}{m}. \quad (3)$$

Its Fourier–Laplace transform [Eq. (8)] provides the link to and the definition of the (complex-valued) memory kernel $\hat{\gamma}(\omega)$,

$$\hat{Z}(\omega) = \frac{k_B T/m}{-i\omega + \hat{\gamma}(\omega)}. \quad (4)$$

Linear response. For a mass m driven by a periodic force $F(t) = F_\omega \cos(\omega t)$ with frequency ω and amplitude F_ω , the stationary response $\bar{\mathbf{v}}(t)$, averaged over many realisations of the experiment, is given by⁶⁷

$$m \frac{d}{dt} \bar{\mathbf{v}}(t) = F(t) - \int_{-\infty}^t m \gamma(t-s) \bar{\mathbf{v}}(s) ds, \quad (5)$$

corresponding to Eq. (1) after shifting the lower integral boundary to $-\infty$ to ensure relaxation of transients. The upper boundary can be shifted to $+\infty$ with the convention that the response function $\gamma(t < 0) = 0$. By linearity of the equation, the solution is of the form $\bar{\mathbf{v}}(t) = \text{Re}[\mathbf{v}_\omega e^{-i\omega t}]$ with complex amplitude \mathbf{v}_ω , and inserting into Eq. (5) yields $\mathbf{v}_\omega = \hat{\gamma}(\omega) F_\omega$ in terms of the generalised mobility,

$$\hat{\gamma}(\omega) := [-i\omega m + m\hat{\gamma}(\omega)]^{-1}, \quad (6)$$

also referred to as complex-valued admittance. Its central ingredient is the one-sided Fourier transform of the response function, $\hat{\gamma}(\omega) := \int_0^\infty e^{i\omega t} \gamma(t) dt$. Comparing to Eq. (4), which describes equilibrium correlations, yields the fluctuation–dissipation relation: $\hat{Z}(\omega) = k_B T \hat{\gamma}(\omega)$.

Friction describes the resistance to a prescribed velocity, as in Stokes’s pendulum experiments¹⁷. Thus, inverting the above argument, the force response to an oscillatory velocity $\mathbf{v}(t) = \mathbf{v}_\omega \cos(\omega t)$ has complex amplitude $F_\omega = \hat{\gamma}(\omega)^{-1} \mathbf{v}_\omega$, and we identify $\hat{\gamma}(\omega)^{-1}$ as a generalised friction. However, merely the real part describes dissipation and deserves to be called a friction, which is seen from the mean dissipated power:

$T_p^{-1} \int_0^{T_p} \mathbf{v}(t) \cdot F(t) dt = \text{Re}[\hat{\gamma}(\omega)^{-1}] |\mathbf{v}_\omega|^2 / 2$, averaged over a full cycle of length $T_p = 2\pi/\omega$. Thus, we set the dynamic friction as

$$\zeta(\omega) := \text{Re}[\hat{\gamma}(\omega)^{-1}] = m \text{Re} \hat{\gamma}(\omega); \quad (7)$$

in particular, $\zeta(\omega) \geq 0$. This is in line with the conventional (Markovian) Langevin equation, $\dot{\mathbf{p}}(t) = -(\zeta_0/m) \mathbf{p}(t) + \boldsymbol{\xi}(t)$. There, the response is governed by $\hat{\gamma}(\omega) = [-i\omega m + \zeta_0]^{-1}$, implying a static friction, $\zeta(\omega) = \zeta_0$.

Equations (6) and (7) (and variants thereof) are the basis of (passive) microrheology experiments^{18–21}, which use observations of Brownian motion to infer the friction $\zeta(\omega)$ and $\text{Im} \hat{\gamma}(\omega)$ of a probe particle in a complex medium and relate it via the GSER to the local visco-elastic properties. The macroscopic shear viscosity, $\eta_0 = (k_B T)^{-1} \int_0^\infty C_\Pi(t) dt$, is the Green–Kubo integral of the autocorrelation, $C_\Pi(t) = \langle \delta\Pi^\perp(t) \delta\Pi^\perp(0) \rangle / V$, of shear stress fluctuations $\delta\Pi^\perp(t)$, given as an off-diagonal element of the stress tensor¹⁶; V denotes the sample volume. Similarly by a fluctuation–dissipation relation, the frequency-dependent response coefficient $\hat{\eta}(\omega)$ to oscillatory shear is the Fourier–Laplace transform [Eq. (8)] of $C_\Pi(t)/k_B T$, and thus $\hat{\eta}(\omega \rightarrow 0) = \eta_0$.

Mathematical framework. For the harmonic analysis of the autocorrelation function $C(t)$ of a stationary time series, we use the Fourier–Laplace transform

$$\hat{C}(z) = \int_0^\infty e^{izt} C(t) dt, \quad (8)$$

which is well-defined for all frequencies z in the upper complex plane, $\mathbb{C}_+ = \{z | \text{Im } z > 0\}$. Along the imaginary axis, $z = iy$, it recovers the conventional Laplace transform. For real frequencies ω , the real and imaginary parts of $\hat{C}(\omega)$ describe physically accessible spectra, which are related to each other by Kramers–Kronig integrals^{52,67}; for example, $\text{Re } \hat{C}(\omega)$ for fixed ω is determined by the full function $\text{Im } \hat{C}(\omega)$. The real part is positive, $\text{Re } \hat{C}(\omega) \geq 0$, and most importantly, we have the unique Fourier backtransform:

$$C(t) = \frac{1}{\pi} \int_{-\infty}^\infty e^{-i\omega t} \text{Re } \hat{C}(\omega) d\omega. \quad (9)$$

If $C(t)$ is n -times continuously differentiable at $t = 0$, this implies sum rules for the spectrum ($k = 0, 1, \dots, n$):

$$\frac{1}{\pi} \int_{-\infty}^\infty (-i\omega)^k \text{Re}[\hat{C}(\omega)] d\omega = C^{(k)}(0) < \infty. \quad (10)$$

In equilibrium, only positive frequencies are needed as $\text{Re } \hat{C}(\omega) = \text{Re } \hat{C}(-\omega)$, and the integrals are real-valued.

Next, we introduce a memory function of $C(t)$ solely by invoking results from complex analysis⁶⁸. $\hat{C}(z)$ as above is a holomorphic function with $\text{Re } \hat{C}(z) \geq 0$, i.e., $i\hat{C}(z)$ is of Herglotz–Nevanlinna type, and $(\text{Im } z) |\hat{C}(z)|$ is bounded in \mathbb{C}_+ . Suppose that $C(t)$ has a regular short-time expansion, $C(t \rightarrow 0) \simeq C_0 [1 - \nu t - \frac{1}{2} a t^2]$, which implies

$$\hat{C}(z) \simeq C_0 (-iz)^{-1} - \nu C_0 (-iz)^{-2} - a C_0 (-iz)^{-3} \quad (11)$$

for large frequencies, $|z| \rightarrow \infty$ with $|\arg z| > \delta$ for some $\delta > 0$. Under these mild requirements, one shows⁶⁸: For given $\hat{C}(z)$ there is a unique memory kernel $\hat{M}(z)$ such that

$$\hat{C}(z) = \frac{C_0}{-iz + \hat{M}(z)} \quad (12)$$

with $i\hat{M}(z)$ of Herglotz–Nevanlinna type and $\hat{M}(z) \simeq \nu + a/(-iz)$ as $|z| \rightarrow \infty$. In particular, $\hat{M}(z)$ corresponds to the autocorrelation function of another (a priori unknown) observable. Iterating the argument yields the continued-fraction representation of $\hat{C}(z)$, well-known from the Zwanzig–Mori projection formalism¹⁶.

In the context of the VACF, one puts $C_0 = v_{\text{th}}^2$, $\nu = 0$, and $a = \omega_0^2$ and infers for the memory kernel $\hat{M}(z) =: \hat{\gamma}(z)$ that $\text{Re } \hat{\gamma}(z) \geq 0$ and $\hat{\gamma}(z) \simeq \omega_0^2/(-iz)$ as $|z| \rightarrow \infty$. This justifies Eq. (4) independently of the notion of a GLE, after taking z along the real line.

By means of Eq. (9), $\hat{\gamma}(z)$ specifies the memory function $\gamma(t)$, which has a physical interpretation as the autocorrelator of the fluctuating acceleration $\xi(t)/m$ in Eq. (1), divided by v_{th}^2 . At low frequencies, $m\hat{\gamma}(z \rightarrow 0) = \zeta_0$ implies a Green–Kubo relation for the hydrodynamic friction:

$$\zeta_0 = m \int_0^\infty \gamma(t) dt. \quad (13)$$

Short-time expansion. The smoothness of physical molecular trajectories, being solutions to Newton’s equations, allows for a short-time expansion of the VACF. Combining with the time-reversal symmetry in equilibrium, $Z(t) = Z(-t)$, only even powers in t contribute and one obtains $Z(t \rightarrow 0) \simeq k_B T \sum_{k=0}^\infty c_k t^{2k}/(2k)!$ with Taylor coefficients c_k given from equilibrium matrix elements of powers of the underlying Liouville operator⁵². To connect with the notation of the main text, $c_0 = 1/m$, $c_1/c_0 = -\omega_0^2$, and we put $c_2/c_0 =: \Omega^4$. Fourier–Laplace transforming term by term yields the high-frequency expansion of $\hat{Z}(\omega)$ and thus of $\hat{\gamma}(\omega) = (k_B T)^{-1} \hat{Z}(\omega)$, which is purely imaginary: $\hat{\gamma}(\omega \rightarrow \infty) \simeq \sum_{k=0}^\infty c_k (-i\omega)^{-1-2k} = c_0/(-i\omega) + c_1/(-i\omega)^3 + \dots$. Using Eq. (7), we have $\zeta(\omega) = |\hat{\gamma}(\omega)|^{-2} \text{Re } \hat{\gamma}(\omega)$, which implies that for high frequencies the friction vanishes, $\zeta(\omega) \equiv 0$, at all orders in $\omega \rightarrow \infty$. A similar situation is familiar from calculus text books: $f(x) = e^{-1/x}$ has a Taylor series $f(x) \equiv 0$ at $x = 0$; the radius of convergence is 0.

The expansion of $\hat{\gamma}(\omega)$ can be represented as a continued fraction that has the same large- ω asymptotics up to terms of order ω^{-5} :

$$\hat{\gamma}(\omega) \simeq \frac{1/m}{-i\omega + \frac{\omega_0^2}{-i\omega + \frac{\omega_0^4}{-i\omega + \dots}}}, \quad (14)$$

introducing $\omega_1^2 =: (\Omega^4 - \omega_0^4)/\omega_0^2$ for brevity. This truncation is an excellent description of our data for $\hat{\gamma}''(\omega)$ at high frequencies, with ω_0 and Ω obtained from fits to $Z(t)$, see Fig. 3d–f. For the memory kernel $\hat{\gamma}(\omega)$, one reads off

$$\hat{\gamma}(\omega \rightarrow \infty) = \omega_0^2/(-i\omega) - \omega_0^2\omega_1^2/(-i\omega)^3 + \mathcal{O}(\omega^{-5}), \quad (15)$$

using Eq. (6), implying for the memory function in time domain:

$$\gamma(t \rightarrow 0) = \omega_0^2 [1 - \omega_1^2 t^2/2] + \mathcal{O}(t^4). \quad (16)$$

Long-time tails. In an unbounded fluid, momentum conservation leads to persistent velocity correlations, $Z(t \rightarrow \infty) \simeq v_{\text{th}}^2 (t/\tau_\infty)^{-3/2}$, which was explained in terms of hydrodynamic backflow and diffusion of a momentum vortex^{16,48,49}. The tail induces a small- ω singularity in the frequency domain⁶⁹, which reads for the memory kernel: $m\hat{\gamma}(\omega \rightarrow 0) \simeq \zeta_0 [1 + (\tau_\infty \zeta_0/m) \sqrt{-4\pi i \omega \tau_\infty}]$, using Eq. (4) and the hydrodynamic friction $\zeta_0 =: m\hat{\gamma}(0) = k_B T / \int_0^\infty Z(s) ds$.

In the framework of the creeping flow equations, Stokes found¹⁷

$$m\hat{\gamma}(\omega \rightarrow 0) \simeq 6\pi\eta_0 a (1 + \sqrt{-i\omega\tau_\eta}) - i\omega m_\eta/2 \quad (17)$$

in terms of the vorticity diffusion time τ_η and an effective particle mass m_η ; matching with the previous expression for the asymptote of $\hat{\gamma}(\omega)$, one identifies $\tau_\eta = 4\pi(\zeta_0/m)^2 \tau_\infty^3$. The real part yields the dynamic friction,

$$\zeta(\omega \rightarrow 0) \simeq 6\pi\eta_0 a (1 + \sqrt{\omega\tau_\eta/2}), \quad (18)$$

showing that its macroscopic limit, $\zeta_0 = 6\pi\eta_0 a$, is approached from above as $\omega \rightarrow 0$ (see Fig. 3b). For water and the supercooled liquid, a different type of power-law decay, $Z(t) \sim -t^{-5/2}$, was found (Fig. 3e, f).

For a general long-time tail of the VACF, $Z(t) \sim t^{-\sigma}$ with $\sigma > 1$, the memory function $\gamma(t)$ asymptotically inherits a power-law decay with the same exponent, but of opposite sign⁷⁰:

$$\gamma(t) \simeq -\hat{\gamma}(0)^2 Z(t)/Z(0), \quad t \rightarrow \infty; \quad (19)$$

which follows from Eq. (3) and by invoking a Tauber theorem⁶⁹. Without any adjustable parameter, the prediction is in excellent agreement with our data for $\gamma(t)$ in case of the LJ fluid. Inspection of a few examples (Figs. 4d, e and 5c) suggests that, in order to accommodate the sign change of the tail, the number of zero crossings (knots) in $\gamma(t)$ is increased by one relative to $Z(t)$.

Analytically solvable example. Consider the following analytically tractable model for the VACF:

$$Z(t) = \frac{v_{\text{th}}^2}{1 + (t/\tau)^2}, \quad v_{\text{th}}^2 = k_B T/m, \quad (20)$$

with relaxation time τ and thermal velocity v_{th} (Supplementary Fig. 1d). It favourably combines the physically required smoothness at $t = 0$ and time-reversibility, $Z(t) = Z(-t)$, with a power-law decay at long times, $Z(t \rightarrow 0) \simeq v_{\text{th}}^2 (t/\tau)^{-2}$; in particular, only even powers of t contribute to the short-time expansion: $Z(t \rightarrow 0) \simeq v_{\text{th}}^2 [1 - (t/\tau)^2 + \mathcal{O}(t^4)]$. From the one-sided Fourier transform of $Z(t)$, we obtain the real and imaginary parts of $\hat{Z}(\omega)$ as $\text{Re } \hat{Z}(\omega) = D_\infty e^{-|\omega\tau|}$ and $\text{Im } \hat{Z}(\omega) = D_\infty [e^{-\omega\tau} \text{Ei}(\omega\tau) - e^{\omega\tau} \text{Ei}(-\omega\tau)]/\pi$, being even and odd functions in ω , respectively (Fig. 5a). Here, $\text{Ei}(\cdot)$ denotes the exponential integral, and $D_\infty = v_{\text{th}}^2 \tau \pi/2$ is the long-time limit of the diffusivity, $D(t) = \int_0^t Z(s) ds = v_{\text{th}}^2 \tau \arctan(t/\tau)$. In application of theorem 1.2 by Mimica⁵¹, we confirm that

$$\lim_{\omega \rightarrow \infty} (-\omega)^{-1} \log(\text{Re } \hat{Z}(\omega)) =: \tau_{\text{rc}} \quad (21)$$

yields the radius of convergence, $\tau_{\text{rc}} = \tau$, of the short-time expansion of $Z(t)$; in particular, $\tau_{\text{rc}} > 0$.

Given $Z(t)$, the explicit expression for the complex memory kernel $\hat{\gamma}(\omega)$ and the friction $\zeta(\omega)$ follow from Eqs. (4), (7), see Fig. 5b. The low- and high-frequency asymptotes correspond to $\zeta(\omega \rightarrow 0) \simeq \zeta_0 (1 + |\omega\tau|)$ and $\zeta(\omega \rightarrow \infty) \simeq \zeta_0 (\pi\omega\tau/2)^2 e^{-|\omega\tau|}$, respectively, with $\zeta_0 = k_B T/D_\infty$. The friction attains its maximum $\approx 1.2\zeta_0$ near $\omega_{\text{max}} \approx 0.892\tau^{-1}$ and falls off rapidly for larger ω ; the position of the maximum of $\text{Im } \hat{\gamma}(\omega)$ sets the onset frequency $\omega_c \approx 4.01\tau^{-1}$. The memory function $\gamma(t)$ is obtained numerically from $\zeta(\omega)$ using Eq. (9), with the short- and long-time asymptotes $\gamma(t \rightarrow 0) \simeq 2\tau^{-2} [1 - 5(t/\tau)^2]$ and $\gamma(t \rightarrow \infty) \simeq -(\zeta_0/m)^2 (t/\tau)^{-2}$, respectively (Fig. 5c).

Adapted Filon algorithm. The computation of the frequency-dependent friction requires a robust numerical Fourier transform, for which we developed a physics-enriched version of Filon’s quadrature formula. The goal is to evaluate $\hat{f}(\omega) = \int_0^\infty e^{i\omega t} f(t) dt$ for a function $f(t)$ sparsely sampled on an irregular grid $t_0 = 0, t_1, \dots, t_n$ for an arbitrary set of frequencies (ω) . The idea of Filon’s algorithm is to interpolate $f(t)$ by elementary functions between the grid points (usually parabolas), thereby reducing the Fourier integral to a finite sum of integrals, for which analytic expressions exist. Anticipating that the normal physical decay of correlation functions is exponential, we approximate $f(t) \approx a_k e^{-\gamma_k t}$ in the interval

$[t_k, t_{k+1}]$ with a_k and γ_k fixed by $f(t_k)$ and $f(t_{k+1})$. Then,

$$\hat{f}(\omega) \approx \int_0^{t_f} e^{i\omega t} f(t) dt + \sum_{k=1}^{n-1} \int_{t_k}^{t_{k+1}} a_k e^{(i\omega - \gamma_k)t} dt + \int_{t_n}^{\infty} a_n e^{(i\omega - \gamma_n)t} dt. \quad (22)$$

Spurious low-frequency oscillations of the transform are removed by smoothly truncating the integral at t_f , here by assuming a terminal exponential decay of $f(t)$, which leads to the last term on the r.h.s. of Eq. (22). In order to preserve the short-time properties of $f(t)$ we fit a polynomial in t^2 to the first few data points and solve the integral analytically; this improves the high-frequency behaviour of $\hat{f}(\omega)$.

The dynamic friction $\zeta(\omega)$ and the memory function $\gamma(t)$ are obtained from MSD data as follows (Fig. 2): The timescale-dependent diffusion coefficient, $D(t) := \partial_t \text{MSD}(t)/6$, is obtained from numerical differentiation. In all cases studied, it grows out from zero, has a maximum, and converges slowly towards the long-time diffusion constant $D_\infty = D(t \rightarrow \infty)$, see Supplementary Fig. 1. Using the above algorithm, we compute⁷¹ $\hat{Z}(\omega) = D_\infty - i\omega \int_0^\infty dt e^{i\omega t} [D(t) - D_\infty]$. Then, $\zeta(\omega)$ is given by Eq. (4) and is transformed back to the time domain with the same algorithm [Eq. (9)]; in particular, we use again a smooth, exponential cutoff. In Fig. 5, the numerical procedure is successfully tested against the analytical model with high accuracy.

Deconvolution in time domain. Inversion of the convolution in Eq. (3) yields the memory function $\gamma(t)$ directly⁷², without resorting to the frequency domain. Numerically, it is not easy to obtain accurate and robust results, and a variety of algorithms have been developed, see ref. ³⁶ for a comparative study. The presence of $\hat{Z}(t)$ in Eq. (3) is removed by integration, yielding $Z(t) = Z(0) - \int_0^t ds G(t-s) Z(s)$ with the integrated memory $G(t) := \int_0^t ds \gamma(s)$. Discretising on a uniform time grid, $t_i = i\Delta t$ ($i = 0, 1, \dots$), and employing the trapezoidal rule for the integral, a recursion relation for $G_i := G(t_i)$ with the initial value $G_0 = 0$ follows³⁶:

$$G_i = \frac{1 - Z_i/Z_0}{\Delta t/2} - 2 \sum_{j=1}^{i-1} G_j Z_{i-j}/Z_0, \quad i \geq 1. \quad (23)$$

Going beyond Kowalik et al.³⁶, we introduce a predictor–corrector scheme to stabilise the numerical solutions: In the predictor step, one evaluates G_i^* and G_{i+1}^* from Eq. (23). Afterwards, the weighted average $G_i := (G_{i-1} + 3G_i^* + G_{i+1}^*)/5$ manifests itself as the corrector step. Results for $G(t)$ can be found in the Supplementary Fig. 2. Finally, the memory function $\gamma(t) = \partial_t G(t)$ is obtained by central differences. If one starts from MSD data on a sparse (e.g., geometrically spaced) time grid, a cubic spline interpolation of the MSD in the variable t^2 is suitable to sample $Z(t)$ on a uniform grid of up to 10^5 points.

Molecular dynamics simulations. Simulations of liquid water were performed with the GROMACS 5.1 package⁷³ using the SPC/E water model, which was shown to accurately reproduce the linear absorption spectra of water from experiments and ab-initio MD simulations up to frequencies of about 30 THz⁷⁴. The system of 3007 molecules in a cubic box of linear size 4.49 nm was equilibrated at 300 K and 1 bar following standard procedures³⁶. Correlation functions were obtained from an constant-particle-number, constant-volume, constant-energy (NVE) simulation over 275 ps with the velocity-Verlet integrator and a time step of 1 fs, using double floating-point precision to achieve good energy conservation. The frequency-dependent viscosity was computed from additional NVE runs, totalling to 49 ns.

For the other two liquids, we used the massively parallel software *HAL's MD package*⁷⁵ (version 1.0a6), permitting the sampling of dynamic correlations on a sparse time grid and featuring smoothly truncated potentials to virtually eliminate any energy drift. The mono-atomic fluid consists of 10^5 particles interacting pairwise via the LJ potential, $U(r) = 4\epsilon[(r/\sigma)^{-12} - (r/\sigma)^{-6}]$, truncated for $r \geq 2.5\sigma$; a unit of time is defined by $\tau_{\text{LJ}} := \sqrt{m\sigma^2/\epsilon}$. Equilibration in the NVE ensemble at number density $\rho = 0.8\sigma^3$ and thermal energy $k_B T = 1.3\epsilon$ followed the protocol given by Roy et al.⁷⁶. The supercooled liquid was realised by a Kob–Andersen 80:20 binary mixture⁷⁷ of 64,000 LJ beads at $\rho = 1.2\sigma^{-3}$ and $T^* := k_B T/\epsilon = 0.6$, equilibrated over a time span of 9,000 τ_{LJ} , and we traced the species of the larger particles. The chosen temperature is well below the melting point⁷⁸, $T^* \approx 1.03$, and is on the onset of universal scaling behaviour according to mode-coupling theory (MCT)⁴⁰; here, the value of the critical temperature is $T_{\text{MCT}}^* \approx 0.43$.

The simulations generate trajectories $r(t)$ of an ensemble of labelled particles for each fluid; our main observable is the mean-square displacement $\text{MSD}(t) := \langle |r(t) - r(0)|^2 \rangle$ for lag time t . For both liquids, single-particle MSDs were averaged from ten production runs, each over 10^8 integration steps of length 0.001 τ_{LJ} .

Control simulations of a single particle in its pinned cage are based on an equilibrated sample of the LJ fluid with 10^6 particles. MSDs were recorded after equilibration of the mobile particle in its static environment over 100 τ_{LJ} and were averaged over 10^6 different cages, computed in parallel, to remove spurious oscillations. Technically, the setup was realised by making two initially identical copies of the fluid interact with each other: the first copy contains the immobile matrix, the second one the tracers (not interacting with each other).

Data availability

The data sets generated and analysed during the current study are available from the corresponding author upon reasonable request.

Code availability

Primary data were generated with open source software as indicated in the “Methods” section. The source code used to analyse the data for the current study is available from the corresponding author upon reasonable request.

Received: 25 November 2019; Accepted: 25 May 2020;

Published online: 10 July 2020

References

1. Franosch, T. et al. Resonances arising from hydrodynamic memory in Brownian motion. *Nature* **478**, 8–11 (2011).
2. Kheifets, S., Simha, A., Melin, K., Li, T. & Raizen, M. G. Observation of Brownian motion in liquids at short times: instantaneous velocity and memory loss. *Science* **343**, 1493–1496 (2014).
3. Berner, J., Müller, B., Gomez-Solano, J. R., Krüger, M. & Bechinger, C. Oscillating modes of driven colloids in overdamped systems. *Nat. Commun.* **9**, 999 (2018).
4. Daldrop, J. O., Kowalik, B. G. & Netz, R. R. External potential modifies friction of molecular solutes in water. *Phys. Rev. X* **7**, 041065 (2017).
5. Guérin, T., Lavernier, N., Bénichou, O. & Voituriez, R. Mean first-passage times of non-Markovian random walkers in confinement. *Nature* **534**, 356 (2016).
6. de Sancho, D., Sirur, A. & Best, R. B. Molecular origins of internal friction effects on protein-folding rates. *Nat. Commun.* **5**, 4307 (2014).
7. Daldrop, J. O., Kappler, J., Brüning, F. N. & Netz, R. R. Butane dihedral angle dynamics in water is dominated by internal friction. *Proc. Natl Acad. Sci. U.S.A.* **115**, 5169–5174 (2018).
8. Sollich, P., Lequeux, F., Hébraud, P. & Cates, M. E. Rheology of soft glassy materials. *Phys. Rev. Lett.* **78**, 2020–2023 (1997).
9. Mizuno, D., Tardin, C., Schmidt, C. F. & MacKintosh, F. C. Nonequilibrium mechanics of active cytoskeletal networks. *Science* **315**, 370–373 (2007).
10. Winter, D., Horbach, J., Virnau, P. & Binder, K. Active nonlinear microrheology in a glass-forming Yukawa fluid. *Phys. Rev. Lett.* **108**, 028303 (2012).
11. Höfling, F. & Franosch, T. Anomalous transport in the crowded world of biological cells. *Rep. Prog. Phys.* **76**, 046602 (2013).
12. Secchi, E. et al. Massive radius-dependent flow slippage in carbon nanotubes. *Nature* **537**, 210–213 (2016).
13. Perakis, F. et al. Coherent X-rays reveal the influence of cage effects on ultrafast water dynamics. *Nat. Commun.* **9**, 1917 (2018).
14. Gaspard, P. et al. Experimental evidence for microscopic chaos. *Nature* **394**, 865–868 (1998).
15. Bartsch, A., Rätzke, K., Meyer, A. & Faupel, F. Dynamic arrest in multicomponent glass-forming alloys. *Phys. Rev. Lett.* **104**, 195901 (2010).
16. Hansen, J.-P. & McDonald, I. *Theory of Simple Liquids* (Academic Press, Amsterdam, 2006).
17. Stokes, G. G. On the effect of the internal friction of fluids on the motion of a pendulum. *Trans. Camb. Philos. Soc.* **9**, 8 (1851).
18. Mason, T. G. & Weitz, D. A. Optical measurements of frequency-dependent linear viscoelastic moduli of complex fluids. *Phys. Rev. Lett.* **74**, 1250–1253 (1995).
19. Gittes, F., Schnurr, B., Olmsted, P. D., MacKintosh, F. C. & Schmidt, C. F. Microscopic viscoelasticity: shear moduli of soft materials determined from thermal fluctuations. *Phys. Rev. Lett.* **79**, 3286–3289 (1997).
20. Squires, T. M. & Mason, T. G. Fluid mechanics of microrheology. *Annu. Rev. Fluid Mech.* **42**, 413–438 (2010).
21. Waigh, T. A. Advances in the microrheology of complex fluids. *Rep. Prog. Phys.* **79**, 074601 (2016).
22. Rigato, A., Miyagi, A., Scheuring, S. & Rico, F. High-frequency microrheology reveals cytoskeleton dynamics in living cells. *Nat. Phys.* **13**, 771–775 (2017).
23. Dorfman, R. *An Introduction to Chaos in Nonequilibrium Statistical Mechanics* (Cambridge University Press, 2003).
24. Cohen, E. G. D. Transport coefficients and Lyapunov exponents. *Phys. A* **213**, 293–314 (1995).
25. Posch, H. A. & Hoover, W. G. Lyapunov instability of dense Lennard-Jones fluids. *Phys. Rev. A* **38**, 473–482 (1988).
26. Zwanzig, R. Time-correlation functions and transport coefficients in statistical mechanics. *Annu. Rev. Phys. Chem.* **16**, 67–102 (1965).
27. Mori, H. Transport, collective motion, and Brownian motion. *Prog. Theor. Phys.* **33**, 423–455 (1965).

28. Forster, D., Martin, P. C. & Yip, S. Moment method approximation for the viscosity of simple liquids: Application to argon. *Phys. Rev.* **170**, 160–163 (1968).
29. Ailawadi, N. K., Rahman, A. & Zwanzig, R. Generalized hydrodynamics and analysis of current correlation functions. *Phys. Rev. A* **4**, 1616–1625 (1971).
30. Bocquet, L., Piasecki, J. & Hansen, J.-P. On the Brownian motion of a massive sphere suspended in a hard-sphere fluid. I. Multiple-time-scale analysis and microscopic expression for the friction coefficient. *J. Stat. Phys.* **76**, 505–526 (1994).
31. Shin, H. K., Kim, C., Talkner, P. & Lee, E. K. Brownian motion from molecular dynamics. *Chem. Phys.* **375**, 316 – 326 (2010).
32. Gottwald, F., Karsten, S., Ivanov, S. D. & Kühn, O. Parametrizing linear generalized Langevin dynamics from explicit molecular dynamics simulations. *J. Chem. Phys.* **142**, 244110 (2015).
33. Lesnicki, D., Vuilleumier, R., Carof, A. & Rotenberg, B. Molecular hydrodynamics from memory kernels. *Phys. Rev. Lett.* **116**, 147804 (2016).
34. Jung, G., Hanke, M. & Schmid, F. Iterative reconstruction of memory kernels. *J. Chem. Theory Comput.* **13**, 2481–2488 (2017).
35. Meyer, H., Voigtmann, T. & Schilling, T. On the non-stationary generalized Langevin equation. *J. Chem. Phys.* **147**, 214110 (2017).
36. Kowalik, B. et al. Memory-kernel extraction for different molecular solutes in solvents of varying viscosity in confinement. *Phys. Rev. E* **100**, 012126 (2019).
37. Tassieri, M., Evans, R. M. L., Warren, R. L., Bailey, N. J. & Cooper, J. M. Microrheology with optical tweezers: data analysis. *New J. Phys.* **14**, 115032 (2012).
38. Nishi, K., Kilfoil, M. L., Schmidt, C. F. & MacKintosh, F. C. A symmetrical method to obtain shear moduli from microrheology. *Soft Matter* **14**, 3716–3723 (2018).
39. Fuchs, M., Götze, W. & Mayr, M. R. Asymptotic laws for tagged-particle motion in glassy systems. *Phys. Rev. E* **58**, 3384–3399 (1998).
40. Götze, W. *Complex Dynamics of Glass-Forming Liquids: A Mode-Coupling Theory*. International Series of Monographs on Physics (Oxford University Press, Oxford, 2009).
41. Williams, S. R., Bryant, G., Snook, I. K. & van Meegen, W. Velocity autocorrelation functions of hard-sphere fluids: Long-time tails upon undercooling. *Phys. Rev. Lett.* **96**, 087801 (2006).
42. Peng, H. L., Schober, H. R. & Voigtmann, T. Velocity autocorrelation function in supercooled liquids: Long-time tails and anomalous shear-wave propagation. *Phys. Rev. E* **94**, 060601 (2016).
43. Ackerson, B. J. & Fleishman, L. Correlations for dilute hard core suspensions. *J. Chem. Phys.* **76**, 2675–2679 (1982).
44. Fuchs, M. & Kroy, K. Statistical mechanics derivation of hydrodynamic boundary conditions: the diffusion equation. *J. Phys.: Condens. Matter* **14**, 9223 (2002).
45. Mandal, S., Schrack, L., Löwen, H., Sperl, M. & Franosch, T. Persistent anti-correlations in Brownian dynamics simulations of dense colloidal suspensions revealed by noise suppression. *Phys. Rev. Lett.* **123**, 168001 (2019).
46. van Beijeren, H. Transport properties of stochastic Lorentz models. *Rev. Mod. Phys.* **54**, 195–234 (1982).
47. Höfling, F. & Franosch, T. Crossover in the slow decay of dynamic correlations in the Lorentz model. *Phys. Rev. Lett.* **98**, 140601 (2007).
48. Alder, B. J. & Wainwright, T. E. Velocity autocorrelations for hard spheres. *Phys. Rev. Lett.* **18**, 988–990 (1967).
49. Ernst, M. H., Hauge, E. H. & van Leeuwen, J. M. J. Asymptotic time behavior of correlation functions. *Phys. Rev. Lett.* **25**, 1254–1256 (1970).
50. Arbe, A., Malo de Molina, P., Alvarez, F., Frick, B. & Colmenero, J. Dielectric susceptibility of liquid water: microscopic insights from coherent and incoherent neutron scattering. *Phys. Rev. Lett.* **117**, 185501 (2016).
51. Mimica, A. Exponential decay of measures and Tauberian theorems. *J. Math. Anal. Appl.* **440**, 266–285 (2016).
52. Boon, J. P. & Yip, S. *Molecular Hydrodynamics*. (Dover Publications, Inc., New York, 1991).
53. Frenkel, J. *Kinetic Theory of Liquids*. (Oxford Univ. Press, London, 1946).
54. Schulz, J. C. F., Schlaich, A., Heyden, M., Netz, R. R. & Kappler, J. Molecular interpretation of the non-Newtonian viscoelastic behavior of liquid water at high frequencies. <https://arxiv.org/abs/2003.08309> [physics.flu-dyn].
55. Tarjus, G. & Kivelson, D. Breakdown of the Stokes–Einstein relation in supercooled liquids. *J. Chem. Phys.* **103**, 3071–3073 (1995).
56. Kumar, S. K., Szamel, G. & Douglas, J. F. Nature of the breakdown in the Stokes–Einstein relationship in a hard sphere fluid. *J. Chem. Phys.* **124**, 214501 (2006).
57. Gupta, S. et al. Validity of the Stokes–Einstein relation in soft colloids up to the glass transition. *Phys. Rev. Lett.* **115**, 128302 (2015).
58. Dehaoui, A., Issenmann, B. & Caupin, F. Viscosity of deeply supercooled water and its coupling to molecular diffusion. *Proc. Natl Acad. Sci. U.S.A.* **112**, 12020–12025 (2015).
59. Parmar, A. D. S., Sengupta, S. & Sastry, S. Length-scale dependence of the Stokes–Einstein and Adam–Gibbs relations in model glass formers. *Phys. Rev. Lett.* **119**, 056001 (2017).
60. Mo, J., Simha, A. & Raizen, M. G. Brownian motion as a new probe of wettability. *J. Chem. Phys.* **146**, 134707 (2017).
61. Huang, K. & Szlafarska, I. Effect of interfaces on the nearby Brownian motion. *Nat. Commun.* **6**, 8558 (2015).
62. Bocquet, L. & Barrat, J.-L. Flow boundary conditions from nano- to micro-scales. *Soft Matter* **3**, 685 (2007).
63. Herrera-Delgado, E., Perez-Carrasco, R., Briscoe, J. & Sollich, P. Memory functions reveal structural properties of gene regulatory networks. *PLoS Comput. Biol.* **14**, e1006003 (2018).
64. Hakim, V. & Silberzan, P. Collective cell migration: a physics perspective. *Rep. Prog. Phys.* **80**, 076601 (2017).
65. Kanazawa, K., Sueshige, T., Takayasu, H. & Takayasu, M. Derivation of the Boltzmann equation for financial Brownian motion: Direct observation of the collective motion of high-frequency traders. *Phys. Rev. Lett.* **120**, 138301 (2018).
66. Franzke, C. L. E., O’Kane, T. J., Berner, J., Williams, P. D. & Lucarini, V. Stochastic climate theory and modeling. *WIREs Clim. Change* **6**, 63–78 (2014).
67. Kubo, R., Toda, M. & Hashitsume, N. *Statistical Physics II: Nonequilibrium Statistical Mechanics* (Springer, Berlin, Heidelberg, 1991).
68. Franosch, T. Long-time limit of correlation functions. *J. Phys. A: Math. Theor.* **47**, 325004 (2014).
69. Karamata, J. Neuer Beweis und Verallgemeinerung der Tauberschen Sätze, welche die Laplacesche und Stieltjessche Transformation betreffen. *J. Reine Angew. Math.* **164**, 27–39 (1931).
70. Corngold, N. Behavior of autocorrelation functions. *Phys. Rev. A* **6**, 1570–1573 (1972).
71. Franosch, T., Spanner, M., Bauer, T., Schröder-Turk, G. E. & Höfling, F. Space-resolved dynamics of a tracer in a disordered solid. *J. Non-Cryst. Solids* **357**, 472–478 (2011).
72. Berne, B. J., Tuckerman, M. E., Straub, J. E. & Bug, A. L. R. Dynamic friction on rigid and flexible bonds. *J. Chem. Phys.* **93**, 5084–5095 (1990).
73. Hess, B., Kutzner, C., Van Der Spoel, D. & Lindahl, E. Gromacs 4: algorithms for highly efficient, load-balanced, and scalable molecular simulation. *J. Chem. Theory Comput.* **4**, 435–447 (2008).
74. Carlson, S., Brüning, F. N., Loche, P., Bonthuis, D. J. & Netz, R. R. Exploring the Absorption Spectrum of Simulated Water from MHz to the Infrared. *The Journal of Physical Chemistry A*. <https://doi.org/10.1021/acs.jpca.0c04063> (2020).
75. Colberg, P. H. & Höfling, F. Highly accelerated simulations of glassy dynamics using GPUs: caveats on limited floating-point precision. *Comput. Phys. Commun.* **182**, 1120–1129 (2011).
76. Roy, S., Dietrich, S. & Höfling, F. Structure and dynamics of binary liquid mixtures near their continuous demixing transitions. *J. Chem. Phys.* **145**, 134505 (2016).
77. Kob, W. & Andersen, H. C. Scaling behavior in the β -relaxation regime of a supercooled Lennard-Jones mixture. *Phys. Rev. Lett.* **73**, 1376–1379 (1994).
78. Pedersen, U. R., Schröder, T. B. & Dyre, J. C. Phase diagram of Kob–Andersen-type binary Lennard-Jones mixtures. *Phys. Rev. Lett.* **120**, 165501 (2018).

Acknowledgements

F.H. is indebted to Thomas Franosch for introducing him to the field of complex transport. We benefited from discussions with Lydéric Bocquet, Matthias Fuchs, Julian Kappler, and Klaus Kroy. This research has been funded by Deutsche Forschungsgemeinschaft (DFG, German Research Foundation) through the grant SFB 1114 (project ID: 235221301, subprojects B03 and C01) and under Germany’s Excellence Strategy–MATH+ : The Berlin Mathematics Research Centre (EXC-2046/1)–project ID: 390685689 (subproject EF4-4). Further funding by the European Research Council (ERC Advanced H 2020 Grant “NoMaMemo”) is gratefully acknowledged. Some of the data were produced with the supercomputer “Lise” (HLRN-IV) of the North-German Supercomputing Alliance.

Author contributions

A.S., R.N., and F.H. conceived the project and wrote the manuscript. B.K. and F.H. performed the simulations, and A.S. and F.H. analysed the data. A.S. carried out the analytical work. All authors discussed the results and implications and commented on the manuscript at all stages.

Competing interests

The authors declare no competing interests.

Additional information

Supplementary information is available for this paper at <https://doi.org/10.1038/s42005-020-0389-0>.

Correspondence and requests for materials should be addressed to F.H.

Reprints and permission information is available at <http://www.nature.com/reprints>

Publisher's note Springer Nature remains neutral with regard to jurisdictional claims in published maps and institutional affiliations.



Open Access This article is licensed under a Creative Commons Attribution 4.0 International License, which permits use, sharing, adaptation, distribution and reproduction in any medium or format, as long as you give appropriate credit to the original author(s) and the source, provide a link to the Creative Commons license, and indicate if changes were made. The images or other third party material in this article are included in the article's Creative Commons license, unless indicated otherwise in a credit line to the material. If material is not included in the article's Creative Commons license and your intended use is not permitted by statutory regulation or exceeds the permitted use, you will need to obtain permission directly from the copyright holder. To view a copy of this license, visit <http://creativecommons.org/licenses/by/4.0/>.

© The Author(s) 2020